Investigation of the Parallel Blade-Vortex Interaction at Low Speed

D. D. Seath,* Jai-Moo Kim,† and D. R. Wilson*
University of Texas at Arlington, Arlington, Texas

Low-speed wind-tunnel tests were conducted to investigate the parallel blade-vortex interaction. Flow-visualization tests of vortex generation performed before the pressure tests showed that a well-defined starting vortex was generated by an impulsively pitched wing. Time history of the pressure distribution on a pressure-tapped wing model was acquired as the starting vortex passed over the wing. These pressure tests revealed that a substantial pressure change near the leading edge was induced by the encountering vortex. The effects of vortex proximity, reduced frequency, and maximum pitch angle of the vortex generator on the pressure change were also investigated.

Nomenclature

c	= chord length of instrument wing
c_{vg}	= chord length of vortex generator wing
C_l	= section lift coefficient of instrumented wing
C_p	= pressure coefficient of instrumented wing, $(P-P_\infty)/q$
k	= reduced frequency, $\dot{\alpha}c_{vg}/V_\infty$
P	= local static pressure
P_{ini}	= initial local static pressure
P_{max}	= maximum local static pressure
P_{min}	= minimum local static pressure
P_∞	= freestream static pressure
q	= freestream dynamic pressure
Re	= Reynolds number
T	= time elapsed after vortex generation
V_∞	= freestream velocity
x	= longitudinal distance from instrumented wing leading edge to pressure tap
x_v	= longitudinal distance from instrumented wing leading edge to vortex center
y_v	= vortex generator height above wing
α	= pitch angle of vortex generator
α_{max}	= maximum pitch angle of vortex generator
$\dot{\alpha}$	= pitch rate of vortex generator
μ_∞	= freestream viscosity
Γ	= vortex strength
ρ_∞	= freestream density

Introduction

HELICOPTER rotors, either while hovering or in forward flight, encounter complex rotor flows such as separation, reverse flow, radial flow, aeroelastic response, transonic shocks, rotor wake, and tip vortex-blade interaction.[1] Of these complex rotor flow problems, blade-vortex interaction has been an important research subject in fundamental rotor aerodynamics since it was identified as a helicopter impulsive noise source in addition to the high advancing blade Mach number.[2] The blade-vortex interaction noise is apt to occur when the helicopter is in powered descending motion.[3] To date, the acoustic formulation of the blade-vortex interaction noise has been well developed; however, the complex aerodynamic data for the input to the acoustic formulation are not provided sufficiently. Also, the computational work has improved a number of finite-difference schemes to simulate the blade-vortex interaction. Most of these schemes have modeled two-dimensional flows.[4]

The helicopter rotor blade produces a differential pressure field across the blade in order to support the weight and provide thrust for forward flight. It leaves behind a continuous vortex sheet because of the lift variation along the blade span. This vortex sheet usually rolls up into two concentrated vortices: the tip vortex and the hub vortex. The hub vortex is carried down by the inflow and is relatively far removed from the blade path. Therefore, the blade-vortex interaction with the hub vortex will not occur generally, and only the tip vortex interaction needs consideration.[4]

When a following blade passes close to a tip vortex from a preceding blade, it causes an unsteady aerodynamic load on the rotor that is thought to radiate the blade-vortex interaction noise. The intersection angle between the vortex filament and the blade span of the following blade ranges from 0 to 90 deg. The 0-deg intersection produces the parallel blade-vortex interaction, and the 90-deg intersection produces the perpendicular interaction. The interaction angle appears to be related to the intensity of the acoustic pulse with the low-angle or parallel intersection, producing a more intensive pulse. This phenomenon has been investigated experimentally and analytically for years.[5-9]

Widnall developed a theoretical model for blade-vortex interaction in which the unsteady lift distribution computed on a two-dimensional airfoil passing obliquely over an infinite line vortex was taken as the boundary condition on a finite blade in the calculation of the acoustic far field.[9] With this theoretical model, she showed that an increase in blade-vortex intersection angle decreased the unsteady signal, and the decreased unsteady signal reduced the peak-to-peak pressure of the transient acoustic signal.[10]

Surendriah[5] used a half-wing as a vortex generator and an instrumented rotating blade in a low-speed wind tunnel to investigate blade-vortex interaction. A scaled-up version of Surendriah's test method was performed at the U.S. Army Aeromechanics Laboratories' 7 × 10-ft wind tunnel at NASA Ames Research Center.[4]

In another wind-tunnel simulation, Booth and Yu[11] utilized a sinusoidally oscillating wing for a vortex generator and placed a stationary wing downstream to simulate the advanc-

Presented as Paper 87-1345 at the AIAA 19th Fluid Dynamics, Plasma Dynamics and Lasers Conference, Honolulu, HI, June 8-10, 1987; received July 8, 1987; revision received Aug. 18, 1988.

*Professor of Aerospace Engineering.
†Graduate Research Assistant, Aerospace Engineering Department.

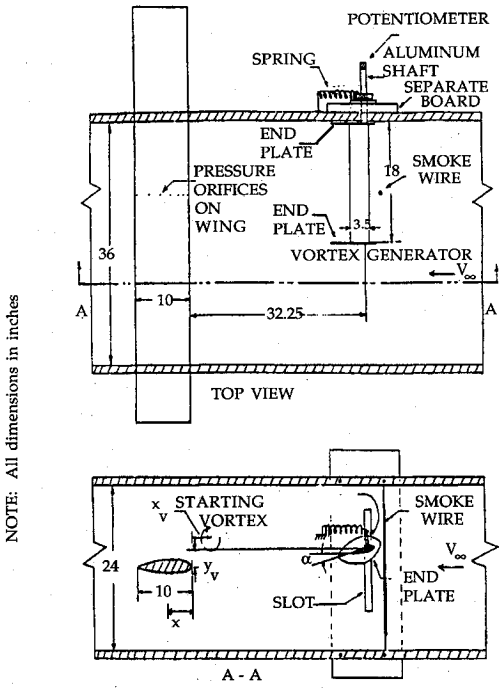

Fig. 1 University of Texas at Arlington low-speed wind-tunnel test setup for blade-vortex interaction (dimensions in inches).

ing rotor blade. The flow visualization study of this test revealed that a pair of vortices was generated from the vortex generator and therefore was not equivalent to an isolated tip vortex encountering a rotor blade.

In the present tests, an impulsively pitched wing in a low-speed wind tunnel was used to generate a starting vortex at its trailing edge. This vortex convected downstream, passed close to an airfoil (blade), and thus simulated the parallel blade-vortex interaction. For a more complete description of the tests, see Kim's thesis.[12]

Experimental Program

The parallel blade-vortex interaction tests were conducted in the University of Texas at Arlington low-speed wind tunnel. The vortex generator consisted of a 3.5-in.-chord, 18-in.-span (NACA 0012 section) half-wing as shown in Fig. 1. Endplates were attached to produce a more uniform spanwise lift distribution. The wing was mounted on a 1.5-in.-diam aluminum shaft at its quarter chord. To rapidly pitch the wing, a spring was connected between the wind-tunnel wall and a moment-arm bolt on the shaft. Two stopper bolts were used to set the initial zero angle and the maximum pitch angle as shown in Fig. 2. The vortex-generator wing was constructed of composite materials to minimize the moment of inertia. The complete vortex generator mechanism was attached to a separate board outside the wind-tunnel wall, which allowed the vortex generator to be moved in the vertical direction. A potentiometer was attached to the end of the shaft to measure pitch angle of the vortex generator. To generate a vortex, the trigger string is pulled down and released.

Downstream of the vortex generator wing, an already existing 6-ft-span, 10-in.-chord wing model (NACA 64A015 section) was mounted across the wind tunnel with both ends extending through wing-section-shaped holes in the side walls (see Fig. 1). This mechanism allowed the wing to be moved in the spanwise direction in order to position chordwise pressure taps installed on the upper and lower surfaces of the wing and connected to 1/16-in.-diam (i.d.), 3-ft-long vinyl tubes extended to outside the wind tunnel. Pressure taps were located at chordwise locations of $x/c = 0$, 0.0125, 0.025, 0.05, 0.1, 0.2, 0.3, 0.4, and 0.7. The wing was at zero angle of attack during all tests.

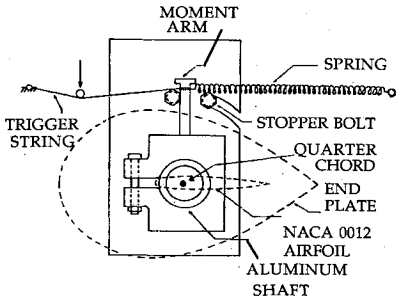

Fig. 2 Schematic diagram of vortex generator.

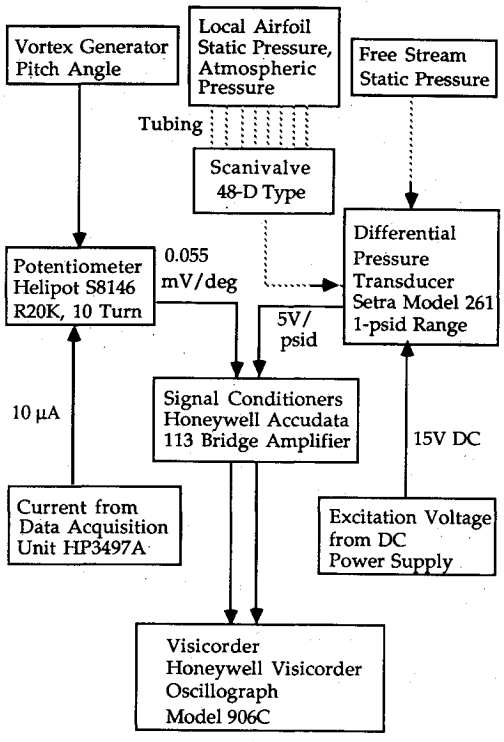

Fig. 3 Data acquisition system.

Pressure measurements on the wing surface were made using a capacitance pressure transducer (SETRA model 261, 1-psid range) connected to a 48-channel Scanivalve. This pressure transducer was calibrated statically using an alcohol manometer for a reference pressure source. Pressure and pitch angle measurements were recorded on an oscillograph (Honeywell Visicorder Oscillograph model 906C). Because only two channels were available on the oscillograph, only one pressure tap at a time was recorded (for each vortex generated), together with the generator pitch angle. Then another pressure tap was connected to the recorder, and the test was repeated. The pitch angle data were used to correlate time among the various tests. The data acquisition system is shown in Fig. 3. Repeated tests showed that pitch angle data were nearly identical.

A smoke wire was placed across the test section upstream of the vortex generator, normal to the spanwise direction and to the freestream flow direction as shown in Fig. 1. Both ends of the smoke wire were connected to a variac, which controlled the input voltage to the smoke wire. The smoke was illuminated by a 120-V, 1000-W flood lamp located downstream of the tunnel diffuser. To observe the generation and movement of the vortex, a 16-mm high-speed (64 frames/s) motion picture camera (Bolex H16 RX-5) loaded with an Eastman Ektakrome Tungsten film was utilized. Reynolds

number during the flow visualization tests was approximately 5100 for the vortex generator and 15,000 for the wing model.

For the pressure tests, the freestream velocity was set at approximately 20, 30, and 40 ft/s to obtain different reduced frequencies (reduced frequency, $k=\dot{\alpha}c_{vg}/V_\infty$) and $\dot{\alpha}$ was kept at 37.9 rad/s, resulting in values of $k=0.55$, 0.37, and 0.28. However, to determine the effect of pitch rate, tests were run with $V_\infty=20$ ft/s and $\dot{\alpha}=30.6$ and 41.1 rad/s, resulting in $k=0.45$ and 0.60, respectively. The vortex generator position was varied vertically with 1-in. increments, and the maximum pitch angle was set at 10, 15, and 20 deg. Right after the Visicorder drive was turned on, the vortex was generated by impulsive pitching. While the vortex passed over the instrumented wing, the surface pressure and the pitch angle were recorded on the Visicorder paper. The pressure source was switched manually with the Scanivalve to the next position, and the procedure was repeated.

The chordwise vortex position was calculated from time history data of pressures with an assumption that the maximum wing surface pressure change at 1.25% chord occurs when the center of the parallel vortex passes over the 1.25% chord position. Another assumption was that the convection velocity of the vortex is equal to the freestream velocity. With these two assumptions, the time axis was rescaled to the chordwise passage of the vortex.

During the pressure tests the Reynolds number varied from 34,000 to 68,000 for the vortex generator and from 100,000 to 200,000 for the wing model. Actual rotor blade Reynolds numbers are on the order of $10\text{–}20\times10^6$.

Results and Discussion

For the flow visualization tests, the wind-tunnel freestream velocity was set at 3 ft/s to generate dense smoke and allow good quality of photographs. The temperature of the smoke wire was controlled by a variac. After the smoke was properly generated, the vortex generator was impulsively pitched from zero to a positve angle of attack to produce the parallel vortex. The generation and convection of the vortex were effectively recorded using the high-speed motion picture camera.

During the flow visualization tests, the 3 ft/s of freestream velocity was calculated from the results of the high-speed motion pictures. The reduced frequency ($k=0.8$) was calculated from the freestream velocity above and the pitch rate, which also was estimated from the high-speed motion pictures.

Sequential pictures of the flow visualization of the vortex generator were copied from the high-speed motion picture film. This motion picture included two types of pitch motion: a pitch-up-and-down motion and a pitch-up-and-hold motion. One endplate was removed to allow better viewing during the motion pictures.

The pitch-up-and-down motion started at $\alpha=0$, pitched up to $\alpha=45$ deg, and immediately back to $\alpha=0$, all in approximately 13/64 s. A starting vortex was observed after about 3/64 s ($\alpha=26$ deg). However, as the pitch continued to increase, a dynamic-stall vortex was also formed and subsequently shed downstream. Because only one vortex was desired, this method of vortex generation was abandoned.

The results of the second generation technique, the pitch-up-and-hold motion, are shown in Fig. 4. The airfoil is pitched up from an initial position (Fig. 4a). After the pitching motion stopped at a low pitch angle (15 deg), a starting vortex formed and shed downstream (Figs. 4b and 4c). At this low incidence angle, a dynamic-stall vortex is not observed.

Viewing the high-speed motion picture revealed that, after the vortex generator wing was pitched up to 15 deg angle of attack, a bending vibration of the wing tip resulted. This vibration was estimated to have an initial amplitude of 0.06 in. at the wing tip, a frequency of 10 Hz, and damped out in four to five oscillations. The effects of this vibration on the wake turbulence are unknown.

A well-defined vortex filament was generated by the pitch-up-and-hold motion. Therefore, this technique was used in the following pressure tests of blade-vortex interaction.

Time histories of wing surface pressures are the basic data in the pressure tests. The effects of vortex height, reduced frequency, and maximum vortex generator angle on the wing surface pressure are investigated.

Figures 5–7 show the time history of chordwise pressure distribution on upper and lower surfaces as the vortex passes over the wing. The freestream velocity was set at approximately 20 ft/s, and the reduced frequency k was calculated from the definition $k=\dot{\alpha}c_{vg}/V_\infty$, where the pitch angle rate $\dot{\alpha}$ was estimated from the pitch data. For example, see Fig. 8, where

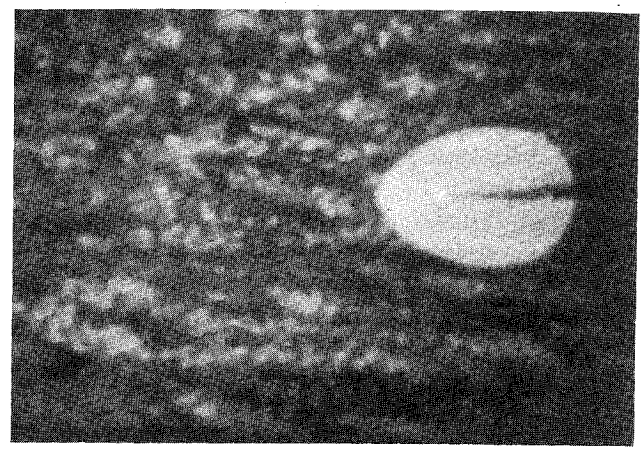

a) Initial position: $\alpha=0$ deg, $T=0$ s

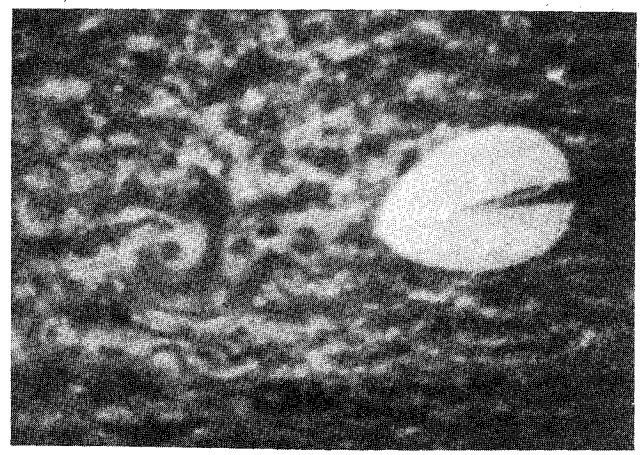

b) $\alpha=15$ deg, $T=14/64$ s

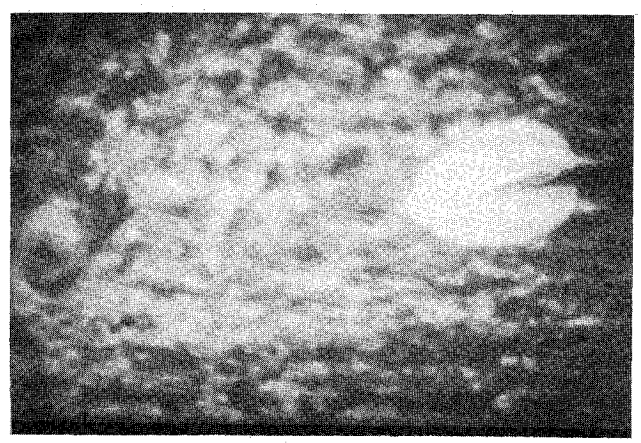

c) $\alpha=15$ deg, $T=23/64$ s

Fig. 4 Smoke flow visualization of pitch-up-and-hold motion of vortex generator.

a vortex generator pitch angle vs time trace is shown. From the measured change in pitch angle $\Delta\alpha = 10$ deg and the time increment $\Delta t = 0.0046$ s, we obtain the pitch rate $\dot{\alpha} = \Delta\alpha/\Delta t = 37.94$ rad/s. In Figs. 5–7 the time axis was rescaled to the longitudinal vortex location with an assumption that the minimum of pressure at $x/c = 0.0125$ occurred when the vortex center passed over it. At the same time, the convection velocity of the vortex was assumed to be equal to the freestream velocity. These figures show that the vortex-induced pressure on the upper surface decreases, since the rotational direction of the starting vortex tends to increase the local velocity by an upwash effect. In the same way, the pressure rise on the lower surface can be explained in that the starting vortex induces a local velocity decrease. Several pressure changes are seen near the leading edge at $x/c = 0.0125$ on upper and lower surfaces. The pressure changes become smaller from approximately $x/c = 0.2$ to the trailing edge. It is shown that the wing surface pressure starts to be influenced by the vortex when it passes upstream of the leading edge near $x/c = -1$, and the effect becomes insignificant when it passes two chord lengths downstream from the trailing edge (at $x/c = 3$). The discrepancy between the initial and final steady pressure in Figs. 5–7 is primarily a result of the downwash induced by the pitched-up vortex generator's bound and trailing vortex system. Repeated tests showed that data repeatability was very good.

Figure 9 shows the effect of vortex proximity to the blade on the wing surface pressure at $x/c = 0.0125$. The time history of pressure at different vortex heights is presented. With an increase in blade-vortex separation, the amount of upwash induced by the vortex is decreased because circumferential velocity falls off with an increase in distance from the vortex center. The decreased upwash reduces the pressure changes on the upper and lower surfaces.

Time history of differential pressure at $x/c = 0.0125$ is depicted in Fig. 10, where the pressure was measured while the freestream velocity was varied from 20 to 40 ft/s. Increasing V_∞ increased $|P - P_\infty|$ because, without the vortex present, the airfoil $|P - P_\infty| = C_p q$. Additional increase in $|P - P_\infty|$ is expected due to the vortex-induced velocity increment, $\Delta v \propto \Gamma/(2\pi r) \propto C_l V_\infty / r$.

The effect of vortex generator reduced frequency on the maximum pressure change at different locations of pressure taps is presented in Fig. 11, where $\Delta C_p = |P_{ini} - P_{min}|/q$ for upper surface and $\Delta C_p = |P_{ini} - P_{max}|/q$ for lower surface. The maximum pressure change increases as the reduced frequency increases over the range tested. For the unflagged symbols the pitch rate $\dot{\alpha}$ was constant at 37.9 rad/s, and the freestream speed was changed from 20 to 40 ft/s. Data for the flagged symbols were obtained with $V_\infty = 20$ ft/s and $\dot{\alpha}$ values of 30.6 and 41.1 rad/s, respectively.

The effect of vortex generator maximum pitch angle on the time history of pressures at two chordwise stations is shown in

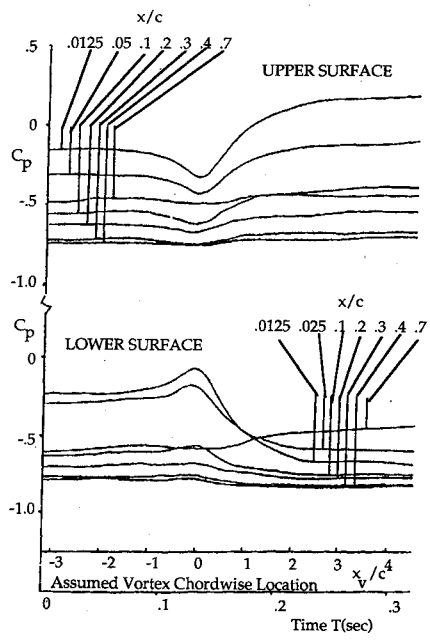

Fig. 5 Time history of pressure coefficient: $V_\infty = 20$ ft/s, $\alpha_{max} = 10$ deg, $k = 0.55$, $y_v/c = 0.18$.

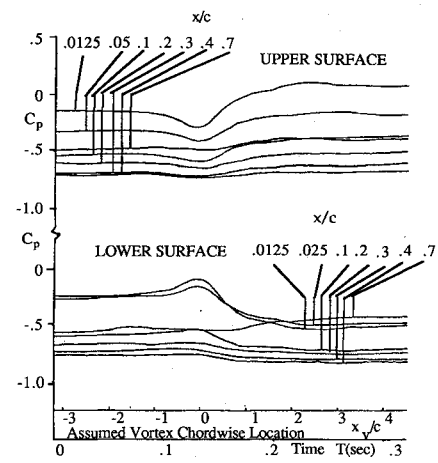

Fig. 6 Time history of pressure coefficient: $V_\infty = 20$ ft/s, $\alpha_{max} = 10$ deg, $k = 0.55$, $y_v/c = 0.28$.

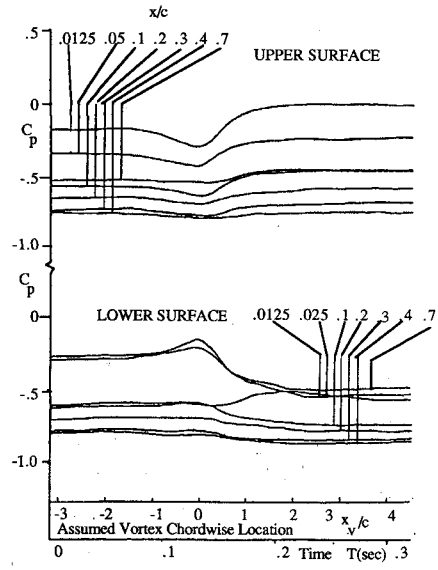

Fig. 7 Time history of pressure coefficient: $V_\infty = 20$ ft/s, $\alpha_{max} = 10$ deg, $k = 0.55$, $y_v/c = 0.38$.

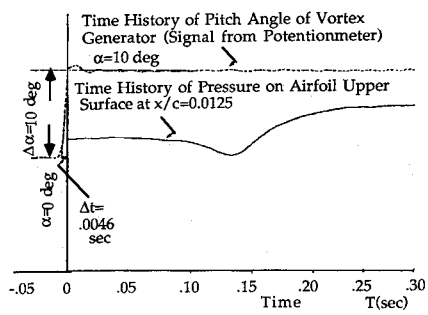

Fig. 8 Time history of pitch angle and pressure.

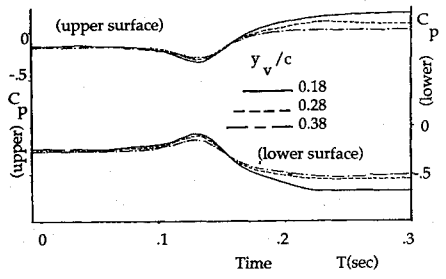

Fig. 9 Time history of C_p at $x/c=0.0125$ as a function of vortex height: $V_\infty=20$ ft/s, $\alpha_{max}=10$ deg, $k=0.55$.

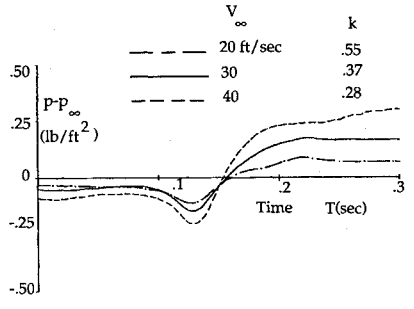

Fig. 10 Time of differential pressure at $x/c=0.0125$ as a function of freestream velocity: $\alpha_{max}=10$ deg, $\dot{\alpha}=37.94$ rad/s, $y_v/c=0.28$, upper surface.

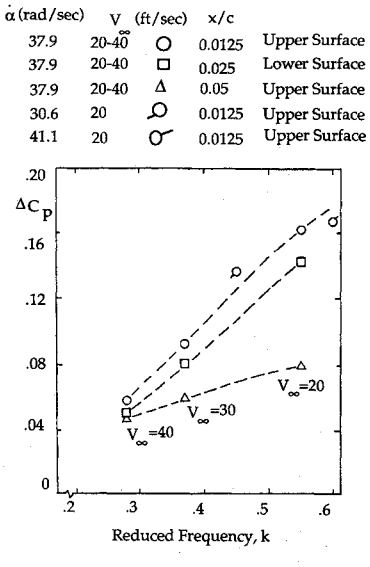

Fig. 11 Vortex-induced pressure change vs reduced frequency of vortex generator; $\alpha_{max}=10$ deg.

Fig. 12. Higher pitch angles induced larger pressure changes because a higher pitch angle produces a larger circulation in the starting vortex. As far as resultant forces are concerned, the bound vortex of proper strength in a uniform stream is equivalent to a body with circulation in a uniform stream. According to circulation theory for two-dimensional flow, the vortex strength Γ can be related to lift coefficient as follows: section lift $=0.5\rho V_\infty^2 c_{vg} C_l=\rho V_\infty \Gamma$. Then, the vortex strength is $\Gamma=0.5\ C_l V_\infty c_{vg}$. The section lift coefficient for an NACA 0012 airfoil is obtained from Ref. 13. For the condition of dynamic stall, the airfoil passes the static-stall angle without significant change in lift-curve slope, as can be seen in Ref. 14. Therefore, the lift coefficient at an angle higher than the static-stall angle can be approximated by linear extrapolation.

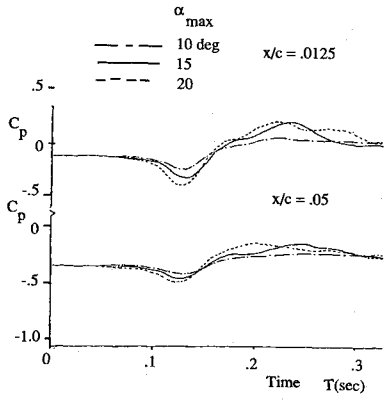

Fig. 12 Time history of C_p at $x/c=0.0125$ and 0.05 as a function of maximum pitch angle of vortex generator: $V_\infty=20$ ft/s, $k=0.55$, $y_v/c=0.28$, upper surface.

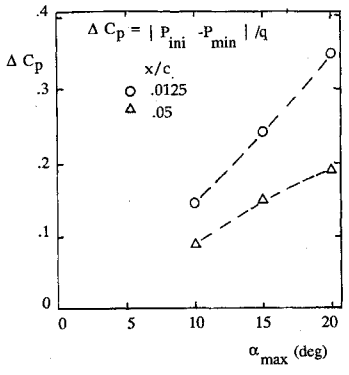

Fig. 13 Vortex-induced pressure changes vs maximum pitch angle of vortex generator: $V_\infty=20$ ft/s, $k=0.55$, $y_v/c=0.28$, upper surface.

Table 1 Estimation of vortex strength of vortex generator: $V_\infty=20$ ft/s, $c_{vg}=3.5$ in.

α, deg	C_l	Γ, ft^2/s
10	1.10	3.20
15	1.65	4.81
20	2.20	6.42

Then, the vortex strength of the vortex generator is estimated as shown in Table 1. This vortex strength appears to be related to the vortex-induced pressure change, as shown in Fig. 13. At higher pitch angles (15–20 deg), a maximum pressure was observed after the pressure experiences a minimum value (see Fig. 12). This appears to be due to the dynamic-stall vortex passing the instrumented wing after the starting vortex. Recalling that the rotational direction of the dynamic-stall vortex is opposite to that of the starting vortex, the dynamic-stall vortex induces a downwash effect opposite to the starting vortex's upwash effect. After the vortices passed downstream, more pressure fluctuations were observed at higher pitch angles. This is probably due to the flow separation wake from the vortex generator at the higher pitch angles.

Figure 14 shows the time history of pressure for two different lengths of tube connected between the orifice and the pressure transducer. The 12-ft-long tube reduces the pressure change up to 60% and also delays the minimum pressure point by 0.016 s compared with the 3-ft-long tube, which was used to obtain all other test data.

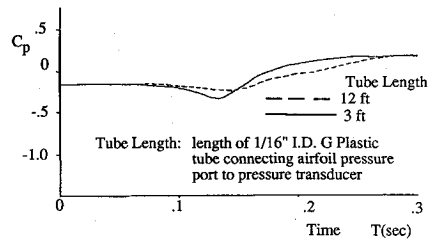

Fig. 14 Time history of C_p for different tube lengths: $V_\infty = 20$ ft/s, $\alpha_{max} = 10$ deg, $k = 0.55$, $y_v/c = 0.18$, $x/c = 0.0125$, upper surface.

Conclusions

A parallel vortex was generated from an impulsively pitched wing in a low-speed wing tunnel. Smoke flow visualization revealed that a well-defined starting vortex was generated when the wing was stopped at a pitch angle of approximately 10 deg.

Blade vortex encounters were measured with a pressure transducer successively connected to the pressure orifices on the downstream airfoil at $\alpha = 0$. Time histories of pressures were recorded for a range of freestream velocities, vortex positions, maximum pitch angles of vortex generator, and reduced frequencies.

Transient pressure changes (pressure drop on upper surface, pressure rise on lower surface) were measured as the vortex passed over the wing. This vortex-induced change is dominant near leading edge. This effect starts when the vortex passes approximately a chord length ahead of the wing and lasts until it passes two chord lengths aft of the trailing edge.

For the range of vortex heights tested, the tests showed that the pressure change increased as the vortex height decreased (passed closer to the wing). The test data also show that the pressure change near the leading edge increased linearly as the reduced frequency of a vortex generator increased over the range of 0.28–0.55. It indicated that a higher reduced frequency produced a stronger vortex, which, in turn, produced a larger pressure change near the leading edge of the wing.

The effect of maximum vortex generator pitch angle on the downstream wing surface pressure change increased as the pitch angle increased from 10 to 20 deg. At the higher pitch angles (15 and 20 deg), a maximum pressure occurred after the pressure experiences a minimum value, which may be caused by a dynamic-stall vortex passing the instrumented wing after the starting vortex. Pressure fluctuations also increase after the vortex travels far downstream. This is probably due to the vortex generator flow separation wake.

Further shortening of the tube length connecting the pressure orifices to the pressure transducer would substantially reduce the response time and improve the accuracy of the quantitative data.

Because of the low Reynolds numbers and Mach numbers of these tests, the data obtained may not be representative of full-scale helicopter BVI, where the blade Reynolds number may be $10\text{–}20 \times 10^6$ or higher, and Mach number may be in the transonic range.

Acknowledgments

This work was supported by a grant from the Army Research Office, Contract DAAG29-84-K-0131, Experimental Simulation of Transonic Vortex-Airfoil Interctions, Thomas L. Doligalski, contract monitor. The Scientific Liaison officer is Hency Jones, U.S. Army Aerostructures Directorate, NASA Langley Research Center, Hampton, Virginia.

References

[1]Davis, S. S., Panel Discussion, Workshop on Blade-Vortex Interactions, NASA Ames Research Center, Oct. 1984.

[2]George, A. R., "Helicopter Noise: State-of-the-Art," *Journal of Aircraft,* Vol. 15, Nov. 1978, pp. 707–715.

[3]Schmitz, F. H., Boxwell, D. A., Lewy, S., and Dahan, C., "Model-to-Full-Scale Comparison of Helicopter Blade-Vortex Interaction Noise," *Journal of the American Helicopter Society,* Vol. 29, April 1984, pp. 16–25.

[4]Caradona, F. S., Laub, G. H., and Tung, C., "An Experimental Investigation of the Parallel Blade-Vortex Interaction," Workshop on Blade-Vortex Interaction, NASA Ames Research Center, Oct. 1984.

[5]Surendriah, M., "An Experimental Study of Rotor Blade-Vortex Interaction," NASA CR-1573, May 1970.

[6]Stepniewski, W. Z., *Rotary-Wing Aerodynamics,* Dover, New York, 1984, pp. 141–232.

[7]Lugt, H. J., *Vortex Flow in Nature and Technology*, Wiley, New York, 1983, pp. 59–66.

[8]Pruyn, R. R. and Alexander, W. T., Jr., "USAALABS Tandem Rotor Airloads Measurement Program," *Journal of Aircraft,* Vol. 4, May–June 1967, pp. 255–260.

[9]Widnall, S. E., "Helicopter Noise Due to Blade-Vortex Interaction," *Journal of the Acoustical Society of America,* Vol. 50, July 1971, pp. 354–365.

[10]Widnall, S. E. and Wolf, T. L., "Effect of Tip Vortex Structure on Helicopter Noise Due to Blade-Vortex Interaction," *Journal of Aircraft,* Vol. 17, Oct. 1980, pp. 705–711.

[11]Booth, E. R. and Yu, J. C., "Two Dimensional Blade-Vortex Interaction Flow Visualization Investigation," AIAA Paper 84-2307, Oct. 1984.

[12]Kim, J.-M., "An Investigation of the Parallel Blade-Vortex Interaction in a Low-Speed Wind Tunnel," M.S. Thesis, Univ. of Texas at Arlington, 1986.

[13]Abbott, I. H. and von Doenhoff, A. E., *Theory of Wing Sections,* Dover, New York, 1959, p. 130.

[14]Carr, L. W., McAlister, K. W., and McCroskey, W. J., "Analysis of the Development of Dynamic Stall Based on Oscillating Airfoil Experiments," NASA TN D-8382, June 1977.